



Complete *n*-hexane oxidation over supported Mn–Co catalysts

S. Todorova^{a,*}, H. Kolev^a, J.P. Holgado^b, G. Kadinov^a, Ch. Bonev^a, R. Pereñíguez^b, A. Caballero^b

^a Institute of Catalysis, Bulgarian Academy of Sciences, Acad. G. Bonchev St., Bldg. 11, 1113 Sofia, Bulgaria

^b Instituto de Ciencia de Materiales and Dpto. Química Inorgánica, CSIC-University of Sevilla, Spain

ARTICLE INFO

Article history:

Received 23 July 2009

Received in revised form 5 October 2009

Accepted 7 October 2009

Available online 30 October 2009

Keywords:

Complete *n*-hexane oxidation

Supported Co–Mn oxide catalysts

ABSTRACT

Two series of Co–Mn samples were prepared by impregnation of silica with aqueous solutions of $\text{Co}(\text{NO}_3)_2 \cdot 6\text{H}_2\text{O}$ and/or $\text{Mn}(\text{NO}_3)_2 \cdot 6\text{H}_2\text{O}$. Cobalt oxide was the predominant phase in one of the series and manganese was used as the promoter. The major component in the second series was manganese oxide and Co was the promoter. The prepared samples were characterized by powder X-ray diffraction (XRD), scanning electron microscopy (SEM), temperature-programmed reduction (TPR), and X-ray photoelectron spectroscopy (XPS) and tested in the reaction of complete *n*-hexane oxidation. The catalytic activity of both single component cobalt and manganese samples was similar, however, a combination between the two elements changed significantly the activity and this depended on the method of preparation. Catalysts prepared by a common solution of Co- and Mn nitrates manifested a considerable increase in activity as a result of very low crystallinity of the supported metal oxide phases, partial enrichment of the surface with cobalt and uniform distribution of oxide agglomerates on the support.

© 2009 Elsevier B.V. All rights reserved.

1. Introduction

The design of a catalytic system for complete oxidation of hydrocarbons is an important problem of environmental catalysis. Supported noble metals, metal oxides and perovskite oxides have been investigated intensely for the combustion of volatile organic compounds (VOCs). The high price of noble metals and their sensitivity to higher temperatures have long motivated investigators to search for substitute catalysis. Metal oxides are an alternative to noble metals as catalysts for complete oxidation. They are less active at low temperatures, but at higher temperatures their activity is similar to that of the noble metals. The most active single metal oxides for combustion of VOCs are the oxides of Cu, Co, Mn, and Ni. Among all metal oxides studied, manganese and cobalt containing catalysts are low cost, environmentally friendly and relatively highly active for VOC combustion. The catalytic properties of MnO_x -based catalysts are attributed to the ability of manganese to form oxides of different oxidation states and to their high oxygen storage capacity (OSC) [1]. Chang and McCarty claim that MnO_x has higher oxygen storage capacity and demonstrates faster oxygen absorption and oxide reduction rates than current commercial ceria-stabilized materials [2]. Appropriate combinations of metal oxides may exhibit higher activity and thermal stability than the single oxides as is recently

published for some cobalt and nickel perovskites [3]. Despite the large number of studies on single component manganese oxides [4–7] and cobalt oxide [8–12] based catalysts, there are only a few works addressed to the catalytic properties of combinations of these two oxides in the combustion reaction of VOCs (e.g. [13,14]). The aim of this study is to establish the influence of the sequence of active component (Co and Mn) introduction on the catalytic activity in complete *n*-hexane oxidation. Hexane has been chosen because it is a component of many products related to industry. In the air it participates in a radical reaction yielding 2-hexanone, 2- and 3-hexyl nitrate and 5-hydroxy-2-pentanone, all of them existing in the photochemical smog.

2. Experimental

2.1. Catalyst preparation

Two series of Co–Mn samples were prepared by impregnation of silica (Aerosil $S_{\text{BET}} = 147 \text{ m}^2/\text{g}$) with aqueous solution of $\text{Co}(\text{NO}_3)_2 \cdot 6\text{H}_2\text{O}$ and/or $\text{Mn}(\text{NO}_3)_2 \cdot 6\text{H}_2\text{O}$ (Table 1). Cobalt oxide is the predominant oxide phase in one of the series, denoted as A, where manganese is used as the promoter. This series involves the following samples: 5Mn + 15Co, 5Mn15Co-MS, 5Mn, and 15Co. Manganese oxide is the main phase in series B, where Co is the promoter. This series includes 5Co + 15Mn, 5Co15Mn-MS, and 15Mn samples. The digits 5 and 15 indicate the respective weight percentage of metal in the catalysts as calculated for the starting solutions. Samples denoted by MS were obtained from a mixed

* Corresponding author. Tel.: +359 2 9792515; fax: +359 2 9712967.

E-mail addresses: todorova@ic.bas.bg, todorova66@yahoo.com (S. Todorova).

Table 1
Sample characterization.

Sample	Metal content ^a		Mean particle size ^b		Lattice parameter 'a' of Co ₃ O ₄ (Å)	Average size of oxide aggregates from SEM (nm)
	Co (wt.%)	Mn (wt.%)	Co ₃ O ₄ (nm)	MnO ₂ (nm)		
Series A						
15Co	14.07		16	n.d.	8.0515	250–1000
5Mn + 15Co	12.93	5.28	15	n.d.	8.0514	200–400
5Mn15Co-MS	15 ^c	5 ^c	7		8.0986	400–600
5Mn	–	5 ^c	–	3		
Series B						
15Mn		12.67	–	16		
5Co + 15Mn	5.64	11.68	n.d.	7		100–500
5Co15Mn-MS	5 ^c	15 ^c	n.d.	6.4		100–200

^a From elemental analysis.^b From XRD data.^c Metal content calculated to be supplied by the starting solutions.

aqueous solution of Co(NO₃)₂·6H₂O and Mn(NO₃)₂·6H₂O. For the 5Mn + 15Co sample, Mn was introduced to calcined 15Co, while in 5Co + 15Mn manganese was deposited first. After each impregnation step the catalysts were calcined at 673 °C for 2 h. Before catalytic measurements the single component samples and the samples prepared from mixed solutions were further calcined for 2 h at the same temperature. Data on sample characterisation are given in Table 1.

2.2. Catalyst characterization

Powder XRD patterns were collected at room temperature in a step-scan regime (step = 0.05°, count time = 2 s) on a Siemens D-501 diffractometer using Cu Kα radiation (λ = 1.5718 Å). XRD data processing was performed by using the X'Pert HighScore program. SEM images were recorded in a field emission scanning electron microscope (FE-SEM) model S5200.

The amount of cobalt in the catalysts was determined by inductively coupled plasma-atomic emission spectroscopy (ICP-AES) on an ARL 3410 instrument. Temperature-programmed reduction (TPR) experiments were carried out from room temperature to 900 °C by equipment described elsewhere [15] using a flow mixture of 5% H₂ in Ar at 10 ml/min and temperature ramp of 10 °C/min. Prior to each run the sample was treated in He for 30 min at 150 °C. XPS measurements were carried out in the UHV chamber of ESCALAB-MkII (VG Scientific) electron spectrometer with a base pressure of about 1 × 10^{−10} mbar (during the measurement 1 × 10^{−9} mbar). The photoelectron spectra were registered using unmonochromatized AlKα (hν = 1486.6 eV) radiation. Passing through a 6-mm slit (entrance/exit) of a hemispherical analyzer, electrons with energy of 20 eV were detected by a channeltron. Because of its low signal for Co2p and Mn2p, pass energy of 50 eV was used. The instrumental resolution measured as the full width at half maximum (FWHM) of the Ag3d_{5/2} photoelectron peak is about 1 eV. The energy scale is corrected to the Si2p-peak maximum at 103.3 eV for electrostatic sample charging. A fitting of the recorded XPS spectra was performed, using a symmetrical Gauss–Lorentzian curve fitting after Shirley-type subtraction of the background.

2.3. Catalytic measurements

n-Hexane oxidation was carried out in a flow type glass reactor at atmospheric pressure with catalyst loading of about 1 cm³ (fraction 0.31–0.63 mm). External mass transfer limitations have been minimized by working at high GHSV (14,400 h^{−1}). The reaction temperature was measured by an internal thermocouple. An inlet *n*-hexane concentration of 2.5 g/m³ was used. The reaction products were analyzed by a Varian 3700 gas chromatograph

equipped with a thermal conductivity detector, a flame ionization detector, and a 3-m column with Porapak Q (0.150–0.180 mm, Riedel-de Haën AG D-3016 Seelze 1) operating at 170 °C. Nitrogen was used as a carrier gas (30 ml/min). All gas lines of the apparatus were heated at 80 °C in order to minimize *n*-hexane adsorption on tube walls. Matheson mass flow controllers were used to keep gas flow rates stable. *n*-Hexane (Fluka) was used both for oxidation and calibration. The gas chromatograph was calibrated against known concentrations of hexane and the decrease in the respective peak areas was used to measure conversion. The conversion was calculated as the ratio of converted to inlet quantity of hexane.

3. Results and discussion

3.1. XRD

3.1.1. Cobalt oxide catalysts with Mn promoter (series A)

As was mentioned above this series includes the 5Mn + 15Co, 5Mn15Co-MS, 5Mn, and 15Co samples. XRD patterns of single and bicomponent samples are shown in Fig. 1. After calcination of the single component 15Co and 5Mn catalysts the main phase is Co₃O₄ and MnO₂, respectively. The peaks at 2θ = 31.37, 36.88, 44.87, 59.39, and 65.29 belong to Co₃O₄ (PDF 01-074-1657). The manganese sample (5Mn) exhibits two diffraction lines at 2θ = 37.33 and 56.8 corresponding to β-MnO₂ (PDF 00-004-0591, pyrolusite). They are broad and have very low intensity owing to the low manganese loading and the high dispersion. According to literature data [16–18], bulk manganese oxides manifest different crystalline phases, depending mainly on the applied temperature and environment of calcination. At low temperatures manganese(IV) oxides can be present in a variety of

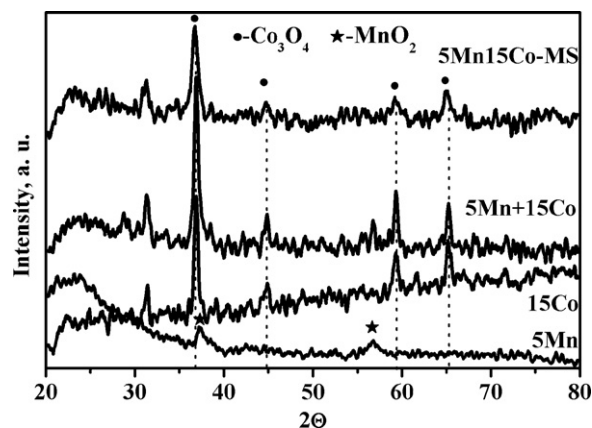


Fig. 1. XRD patterns of series A samples calcined at 400 °C.

structural forms [17], the most stable structure among them being β - MnO_2 [7]. However, the bicomponent samples do not show any XRD lines for MnO_2 or Co–Mn mixed oxides, most probably because the oxide particles are well dispersed on the support. If Mn is added to calcined 15Co the position and intensity of the lines for Co_3O_4 do not change. The cobalt oxide particles size calculated by means of Scherrer equation is the same for these two samples (Table 1). The lattice parameter ‘a’ of Co_3O_4 estimated for the single component 15Co and bicomponent 5Mn + 15Co catalysts (Table 1) is similar and close to the one reported for the Co_3O_4 phase (PDF 01-074-1657, $a = 8.0650 \text{ \AA}$). Some changes are evident in the XRD patterns of the sample prepared from a mixed solution. The Co_3O_4 lines become broader and weaker indicating a smaller Co_3O_4 particle size. Most likely, this effect is due to interaction between cobalt and manganese resulting in a loss of crystallinity. As known that both Co and Mn cations have similar ionic radii and can form stable mixed oxides [19,20], which could explain that the position of the Co_3O_4 reflections appeared at a slightly lower 2θ for catalysts prepared from a mixed solution and also that the lattice parameter increases in comparison with that of pure Co_3O_4 (Table 1). According to El-Shobaky et al. [19] the incorporation of manganese in the lattice of Co_3O_4 is accompanied by the conversion of some Co^{3+} into Co^{2+} . The ionic radius of Co^{2+} is higher than that of Co^{3+} and this causes the increase of the lattice constant. All the mentioned changes in the XRD patterns, particle size and lattice constant can be taken as direct evidence for incorporation of Mn ions in the lattice of Co_3O_4 . Our results are in accordance with those of Morales et al. [20,21]. Using STEM-EELS and EXAFS these authors have established the formation of Co–Mn mixed oxide on TiO_2 support, after deposition of Mn on a dried Co/ TiO_2 sample prepared by deposition-precipitation followed by calcinations where the mixed Co–Mn oxide is not formed if manganese is deposited on a calcined single component cobalt sample prepared by impregnation.

3.1.2. Manganese oxide catalysts with Co promoter (series B)

This series comprises the following samples: 15Mn, 5Co + 15Mn, and 5Co15Mn-MS. The XRD patterns of 15Mn show diffraction lines at $2\theta = 28.9, 37.3, 42.8, 56.8$ consistent with the MnO_2 (PDF-00-004-0779) (Fig. 2). The addition of cobalt to the calcined 15Mn sample results in a shift of the main diffraction lines of MnO_2 to smaller angles and an increase in the cell parameters of the MnO_2 . The cell parameters are $a = 4.3727 \text{ \AA}$, $c = 2.8835 \text{ \AA}$ for 15Mn and $a = 4.3993 \text{ \AA}$, $c = 2.9019 \text{ \AA}$ for 5Co + 15Mn. Since the ionic radii of Co^{2+} (0.78 \AA) and Co^{3+} (0.64 \AA) are higher than that of Mn^{4+} (0.60 \AA) the above-mentioned changes could be regarded as a direct proof of the dissolution of Co ions in the lattice of MnO_2 .

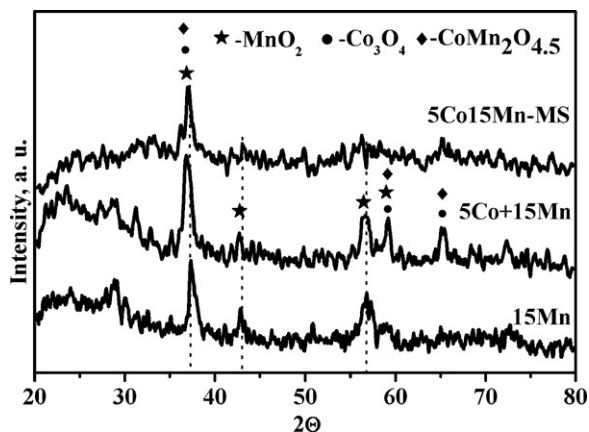


Fig. 2. XRD patterns of series B samples calcined at 400 °C.

Although the formation of mixed $\text{MnCo}_2\text{O}_{4.5}$ oxide has been previously reported [19,20], the analysis of XRD data on Co–Mn oxide systems is difficult because the MnO_2 , Co_3O_4 and $\text{MnCo}_2\text{O}_{4.5}$ compounds demonstrate lines in the XRD patterns at similar 2θ values. In addition, most of the diffraction lines appeared as broad peaks of low intensity in the pattern of the 5Co15Mn-MS sample in accordance with the presence of well-dispersed oxide phase(s). We calculated the mean particle size of MnO_2 in the samples using the reflection at $2\theta = 56.8^\circ$, coming only from the [2 1 1] plane of MnO_2 . The calculated particle size of MnO_2 in the 15Mn sample was 16 nm and decreased to 7 nm after modification with Co (5Co + 15Mn sample). The oxide particle size of the sample prepared from a mixed solution was calculated from the reflection at $2\theta = 37.7$. However, this is not an authentic reflection of MnO_2 because several compounds occur simultaneously on the support and display XRD patterns in this position. For this reason, the value of the calculated particle size is only tentative.

3.2. TPR

3.2.1. Cobalt oxide catalysts with Mn promoter (series A)

Fig. 3 represents the TPR profiles of all samples from series A. The single component 15Co sample exhibits two reduction peaks: one with a maximum at around 340 °C and another with a maximum at 358 °C. These two peaks fit well in the reduction interval of bulk Co_3O_4 powder or large supported Co_3O_4 particles [22]. The peak at 340 °C is attributed to the reduction of Co_3O_4 to CoO and that at 358 °C originates from the reduction of CoO to Co^0 . Hydrogen consumption at 318 and 420 °C is registered with the single component manganese sample. The reduction of Mn oxides is more complex and takes place via different reduction stages. Ferrandon et al. [23] have reported peaks with maxima at 328 and 424 °C during reduction of supported MnO_x assuming that MnO_x is

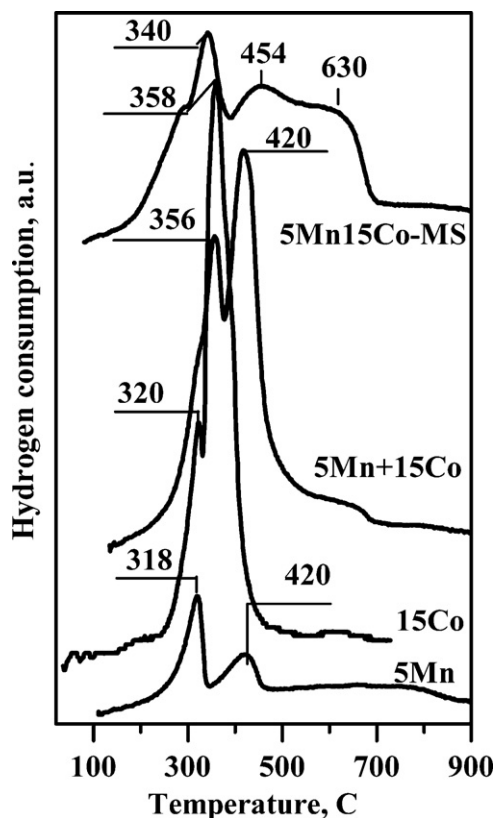


Fig. 3. TPR spectra of single and bicomponent catalysts of series A.

a mixture of MnO_2 and Mn_2O_3 . Kapteijn et al. [24] have observed two peaks during reduction of MnO_2 prepared from nitrates. One peak around 320 °C was attributed to reduction of MnO_2 or Mn_2O_3 to Mn_3O_4 , and another peak at 440 °C was assigned to reduction of Mn_3O_4 to MnO . After reduction the colour of our single component manganese sample was green, which means that the reduction ends at MnO . The O/Mn ratio calculated from H_2 consumption is 2 for the 5Mn catalyst, which is clear evidence that manganese is present as MnO_2 . Following these considerations, we can assign the peaks at 318 and 420 °C to the reduction of finely divided MnO_2 . Addition of Mn to the calcined 15Co sample slightly shifts the peaks from the Co_3O_4 reduction to higher temperatures. This can be ascribed to interaction between MnO_x and Co_3O_4 . The shoulder observed at the low temperature side of the TPR profile is likely a result of MnO_x reduction. The sample prepared from a mixed solution exhibits totally different reduction behaviour. Four overlapping peaks at 286, 340, 454, and 630 °C are observed. As was shown above, the average particle diameter of Co_3O_4 calculated from the powder X-ray pattern of the 5Mn15Co-MS sample is smaller than that in 15Co and 5Mn + 15Co. For this reason, we suggest that the first two peaks come from the reduction of a finely divided Co_3O_4 phase. This could be explained considering a particle size effect: the smaller the particle size, the lower the registered reduction temperature. Okamoto et al. found the same tendency for the reduction of variously sized Co_3O_4 supported on SiO_2 [25]. The reduction of MnO_2 is possible also in this temperature interval. The hydrogen consumption at 450 and 630 °C could be associated with reduction of Co–Mn mixed oxide. Das et al. [26] reported the reduction of pure $(\text{Co}_{1-x}\text{Mn}_x)_3\text{O}_4$ phase at a temperature slightly above 600 °C. Due to the presence of many different phases, which are reduced in the same temperature interval, the quantitative analysis of the TPR profiles of bicomponent catalysts cannot be accurate.

3.2.2. Manganese oxide catalysts with Co promoter (series B)

The TPR profile of the single component 15Mn sample (Fig. 4) shows two peaks at 334 and 424 °C. They are attributed to a two-step reduction of MnO_2 in accordance with reference data [23,24]. The reduction maxima with this sample are found at a higher temperature in comparison with that of single component 5Mn. Larger manganese particles and higher crystallinity of 15Mn are responsible for this effect. In the case of bulk MnO_x not only the oxidation state, but also the crystallinity and/or the concentration of defects determine the reducibility in hydrogen [27]. The O/Mn ratio calculated from H_2 consumption is 1.97 for the 15Mn catalyst, which is clear evidence that manganese occurs as MnO_2 . The TPR data on the bicomponent samples are also in accordance with enhanced consumption of Co in the formation of mixed oxide phase(s) both in the case of consecutive deposition of Mn and Co and from a mixed solution. As it is seen, both peaks due to MnO_2 reduction at 334 and 424 °C are shifted to lower temperatures and decrease in intensity with the bicomponent samples in agreement with higher dispersion of the remaining MnO_2 . This feature is accompanied by the appearance of a broader region of hydrogen consumption in the interval 500–700 °C, which is assumed to be a result of mixed oxide phase(s) reduction. As seen, it is more significant with the 5Co15Mn-MS sample. Our bicomponent samples were prepared by impregnation of the support with nitrates and subsequent calcinations at 400 °C. It was found that decomposition of supported mixed Co–Mn nitrates at low temperature (250–400 °C) often produces a finely divided non-stoichiometric spinel $\text{MnCo}_2\text{O}_{4+\delta}$ [28]. This is a further reason to ascribe hydrogen consumption above 500 °C in the bicomponent samples from series A and B to the reduction of mixed Co–Mn oxides.

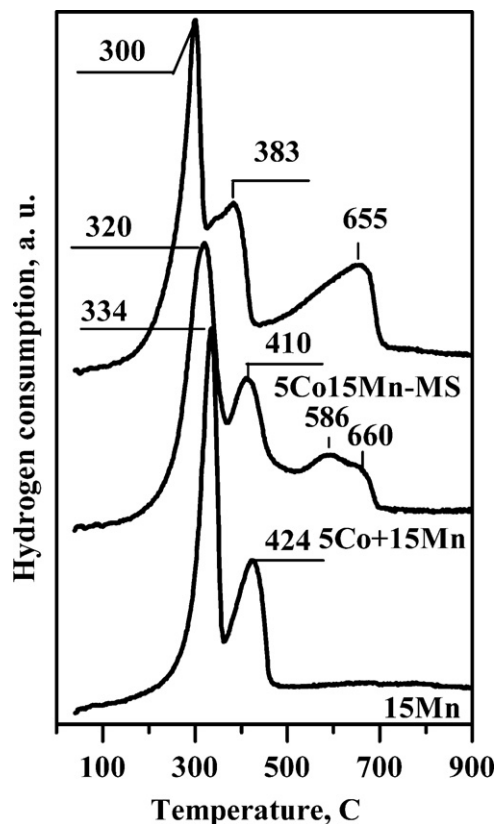


Fig. 4. TPR spectra of single and bicomponent catalysts of series B.

3.3. XPS

3.3.1. Cobalt oxide catalysts with Mn promoter (series A)

XPS spectra in the $\text{Co}2p$ region of series A samples are shown in Fig. 5. The XPS spectrum of the 15Co was fitted assuming that the Co^{2+} to Co^{3+} ratio is 1:2 as in the Co_3O_4 . Since the $2p_{3/2}$ binding energies of Co^{2+} are relatively close to those of Co^{3+} , cobalt oxidation state of two must be distinguished by the presence of a satellite at 3.6–6.5 eV above the main $2p_{3/2}$ line [29,30]. The peak of $2p_{3/2}$ at 779.2 eV and the very low intensity of the $3d \rightarrow 4s$ shake-up satellite peak at 785.2 eV of the 15Co catalysts are characteristic of Co_3O_4 [22,31]. Inspection of fitted XPS spectra of the manganese-modified samples shows that the relative intensity of the Co^{3+} contributions increase more significantly for the catalyst prepared from a mixed solution. Co^{3+} is the major cobalt species in the 5Co15Mn-MS sample. As was mentioned in the Introduction section, MnO_x has high oxygen storage capacity. Most probably, some oxygen species from MnO_2 are incorporated in the cobalt oxide thus increasing the mean oxidation state of Co. The higher intensity of the $\text{Co}2p_{3/2}$ peak can be related to an increase in the cobalt oxide dispersion as was concluded from XRD data. Table 2 gives the Co/Si and Mn/Si atomic ratios and the Co/Mn ratio at the surface and in the bulk. It is seen that the Co/Si ratio of 5Mn15Co-MS is the highest among all samples in this series and that the Co/Mn ratio at the surface is higher than that in the bulk. The Mn/Si atomic ratio of 5Mn15Co-MS is three times lower than that in the single component 5Mn catalyst (Table 2). All these results demonstrate enrichment in the Co component on the surface of the sample prepared from a mixed solution. The decrease in intensity of the $\text{Co}2p_{3/2}$ peak of the 5Mn + 15Co sample is, likely, a result of partial covering of Co by Mn. The mean escape depth of the photoelectrons generated through MnO_2 is only 1.2 nm, implying that a small coverage of manganese oxide on cobalt oxide can significantly reduce the amount of photoelectrons reaching the

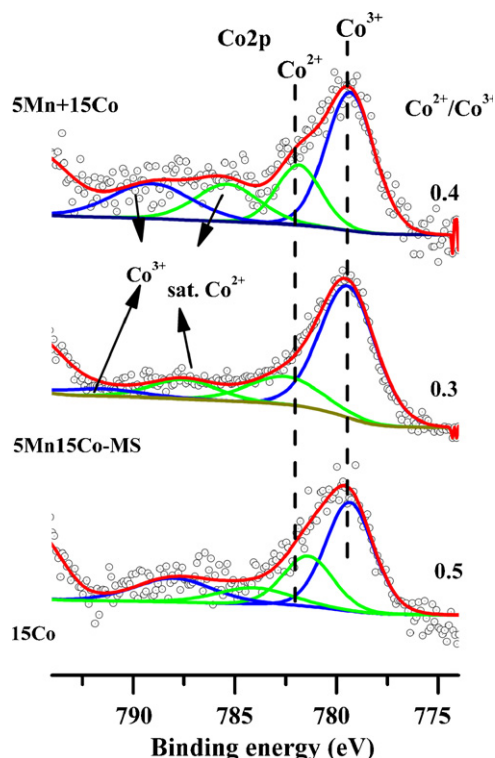


Fig. 5. Fitted Co2p photoelectron peaks of the Co and Mn-Co samples of series A.

Table 2

Active component distribution in the samples as determined by XPS.

Samples	Atomic percent on the surface			Atomic ratios		
	Co	Mn	Co/Mn on the surface	Co/Mn in the bulk	Co/Si	Mn/Si
Series A						
15Co	0.31				0.0086	
5Mn + 15Co	0.1	0.3	0.33	2.2	0.00285	0.0086
5Mn15Co-MS	0.7	0.1	7	2.6	0.0194	0.0027
Series B						
15Mn		0.58				0.0161
5Co + 15Mn	0.2	0.2	0.45	1	0.0057	0.0057
5Co15Mn-MS	0.3	0.6	0.36	0.5	0.00833	0.0166

detector [32]. Consequently, the decrease in the surface Co/Mn atomic ratio can be well explained bearing in mind a partial coverage of the cobalt oxide by manganese oxide. In contrast to the investigation of Morales et al. [20,21], who found that MnO_2 and Co_3O_4 are situated apart after manganese deposition by impregnation on calcined Co/TiO_2 samples, our results show that MnO_2 and Co_3O_4 are closely related.

Fig. 6 presents XPS spectra in the Mn2p region for all the prepared samples of series A. The binding energy of $\text{Mn}2p_{3/2}$ of the single component sample is 641.7 eV and the spin orbital splitting is $\Delta E = 11.7$ eV. These values are in the range of those reported for MnO_2 (641.7–642.2 eV, $\Delta E = 11.7$ eV) [28,31]. As was shown above, according to XRD and TPR data Mn is in the form of MnO_2 in the single component sample. As can be seen from Fig. 6 the $\text{Mn}2p_{3/2}$ peak shifts to lower binding energy in the bicomponent samples and this shift could be ascribed to the occurrence of Mn^{3+} . One can assume the presence of Mn^{3+} because in the $\text{Mn}_x\text{Co}_{3-x}\text{O}_4$ system the oxidation states of +3 or +4 of Mn have been proposed for a ratio that depends on the preparation method [33,34]. The binding energy of Mn_2O_3 has been reported in

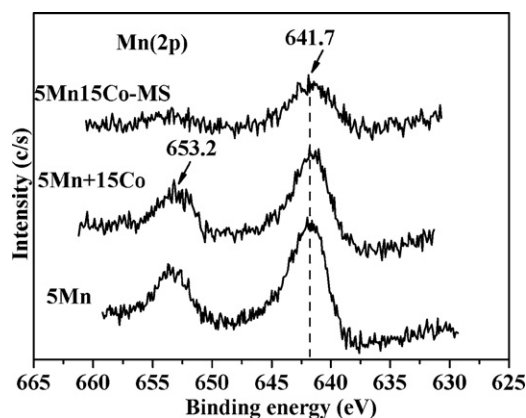


Fig. 6. XPS spectra of Mn2p region of series A Mn-Co samples.

the range 641.5–641.7 eV [26,31]. It should be noted that the binding energies of various Mn ions have very close values and, consequently, it is difficult to distinguish between various oxidation states of Mn [35,36]. The fact that the $\text{Mn}2p_{3/2}$ peak is very broad may imply co-existence of Mn^{3+} and Mn^{4+} ions at the catalyst surface. The lower intensity of the peaks of the sample prepared from a mixed solution is in accordance with a lower manganese concentration on the surface. As was mentioned above, the Mn/Si ratio was three times lower for the 5Mn15Co-MS sample in comparison with the single component Mn catalyst.

3.3.2. Manganese oxide catalysts with Co promoter (series B)

Fig. 7 displays XPS spectra in the Co2p region of series B samples. The photoelectron peaks of a single component cobalt sample with cobalt loading of 5 wt.% are given for comparison, as well. The binding energy at 780.2 eV and a $2p_{3/2}$ – $2p_{1/2}$ splitting of 15.2 eV are characteristic of octahedral Co^{3+} [22,31]. The presence of a peak at 780 eV and a satellite at about 787.6 eV in the photoelectron spectrum of the 5Co + 15Mn sample indicates that surface cobalt is a Co(II) species. For the

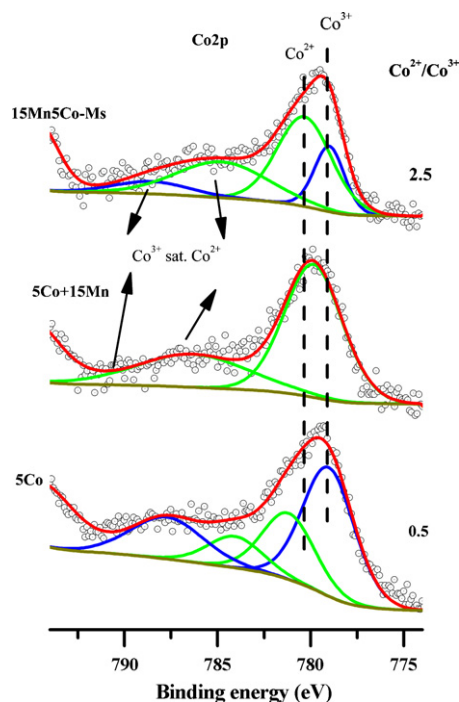


Fig. 7. Fitted Co2p photoelectron peaks of series B Co and Mn-Co samples.

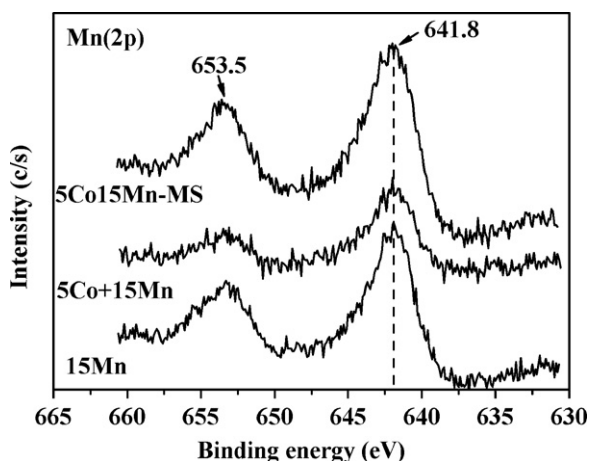


Fig. 8. XPS spectra of Mn2p region of series B Co and Mn–Co samples.

sample prepared from a mixed solution of the respective salts (5Co15Mn-MS), Co^{2+} is the major species ($\text{Co}^{2+}/\text{Co}^{3+} = 2.5$). So, in contrast to series A samples the cobalt in series B is present mainly as Co^{2+} . The XPS spectra in the Mn2p region of the samples from series B are given in Fig. 8. Like the samples of series A the binding energy of the XPS $\text{Mn}2p_{3/2}$ is in the range typical of MnO_2 (641.7–642.2 eV). It was already shown above by TPR and XRD that manganese occurs as MnO_2 in the single component sample. The presence of Mn^{3+} cannot be excluded especially in the bicomponent catalysts, because of the easy formation of solid solutions between cobalt and manganese. The $\text{Mn}2p_{3/2}$ peaks are rather broad and the BE shifts are not resolved well enough to quantify the relative contribution of different manganese oxides. The higher intensity of the $2p_{3/2}$ peak of the 5Co15Mn-MS sample could be related to an increase in the Mn dispersion as was concluded from XRD data (Table 1). The Mn/Si ratio is the highest among the samples in this series (Table 2).

3.4. SEM

Figs. 9 and 10 present SEM images from backscattered electrons of the samples from series A (15Co, 5Mn + 15Co and 5Mn15Co-MS). SEM images of the samples from series B are shown in Fig. 11. The obtained images are dependent on atomic number contrasts among the different constituents of the sample. Bright zones represent heavy elements, while dark zones correspond to the light elements. Thus, the bright zones can be assumed to stand for the supported species (manganese and/or cobalt) and the dark ones are due to the silica. Because of the very close atomic numbers of Co and Mn it is not possible to differentiate between them. The mean particle size of the oxide agglomerates are given in Table 1. The single component cobalt catalyst is composed by large irregular particles, of about 0.2–1 μm in size, scattered on the siliceous surface. It is seen that manganese-modified samples show more uniform distribution of the oxide agglomerates (200–400 nm for 5Mn + 15Co and 400–600 nm for 5Mn15Co-MS). The SEM images demonstrate the smallest crystal agglomerates (100–200 nm in size) with the 5Co15Mn-MS sample (Fig. 11).

Based on the results discussed above it can be concluded that:

- The manganese oxide partially covers cobalt oxide particles in the sample prepared by deposition of Mn on the calcined 15Co sample. The average size of the Co_3O_4 particles does not change after manganese deposition. There is no data on mixed Co–Mn oxide formation.
- The addition of Co to the calcined 15Mn sample results in the partial dissolution of cobalt in the lattice of MnO_2 and the formation of mixed oxide phases. The surface cobalt is in the second oxidation state (Co^{2+}).
- The main conclusions that can be drawn from the results obtained with the Co–Mn catalysts prepared from a mixed solution are: (i) Formation of finely divided oxide (cobalt or manganese), which is reduced at a lower temperature. (ii) Enrichment in Co on the surface. Cobalt in manganese-promoted cobalt catalysts (series A) occurs on the support mainly as Co^{3+} , while promoting cobalt in

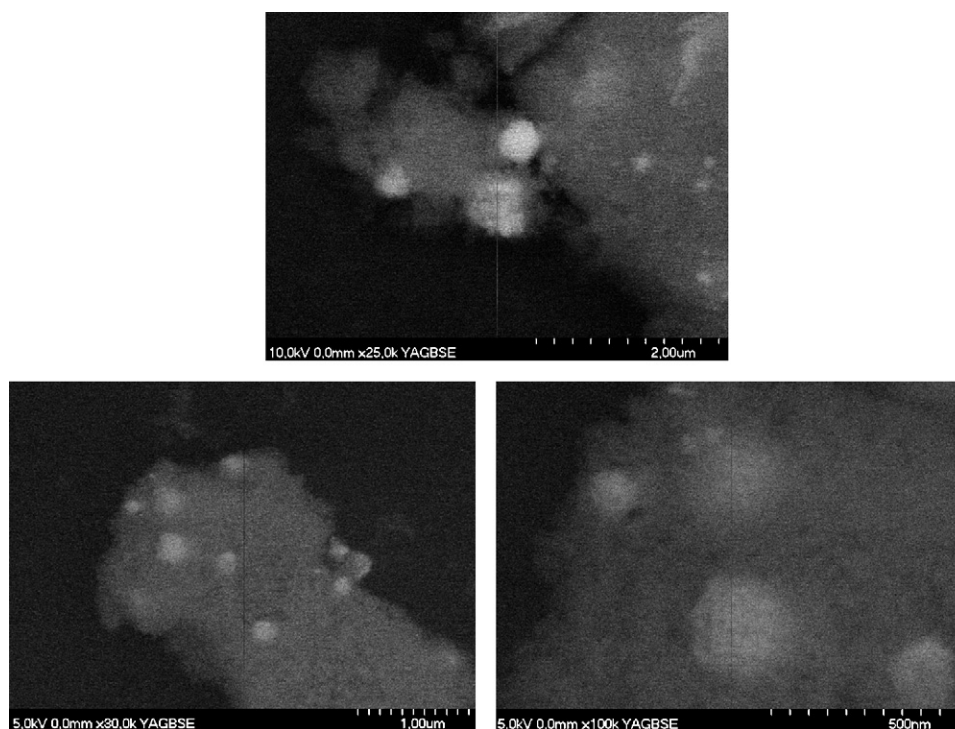


Fig. 9. SEM images of the 15Co sample.

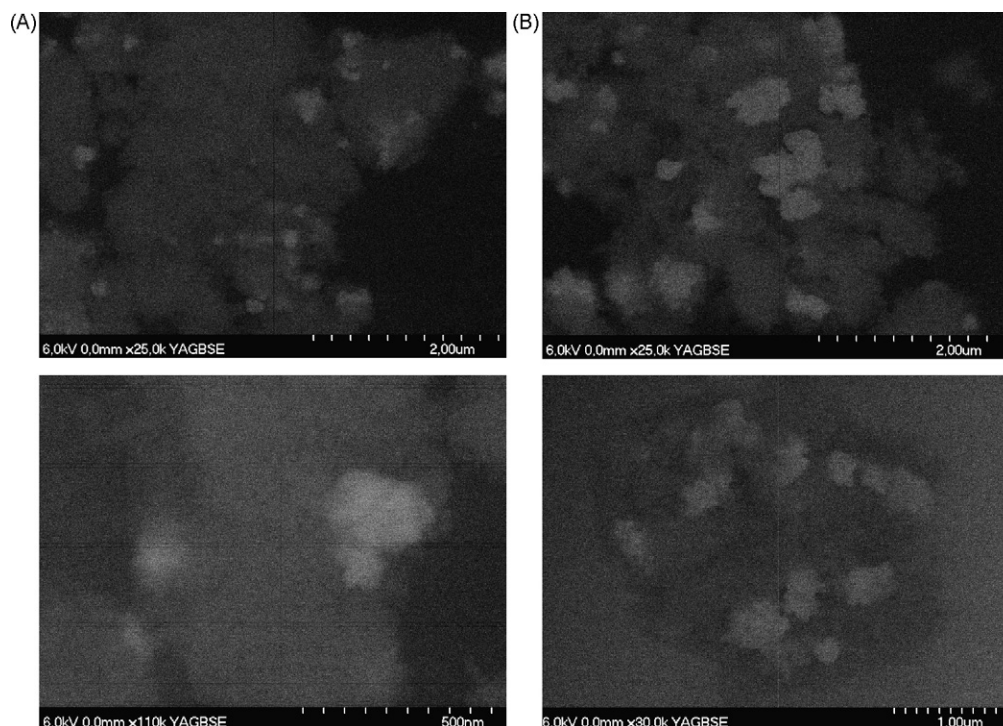


Fig. 10. SEM images of (A) 5Mn + 15Co and (B) 5Mn15Co-MS.

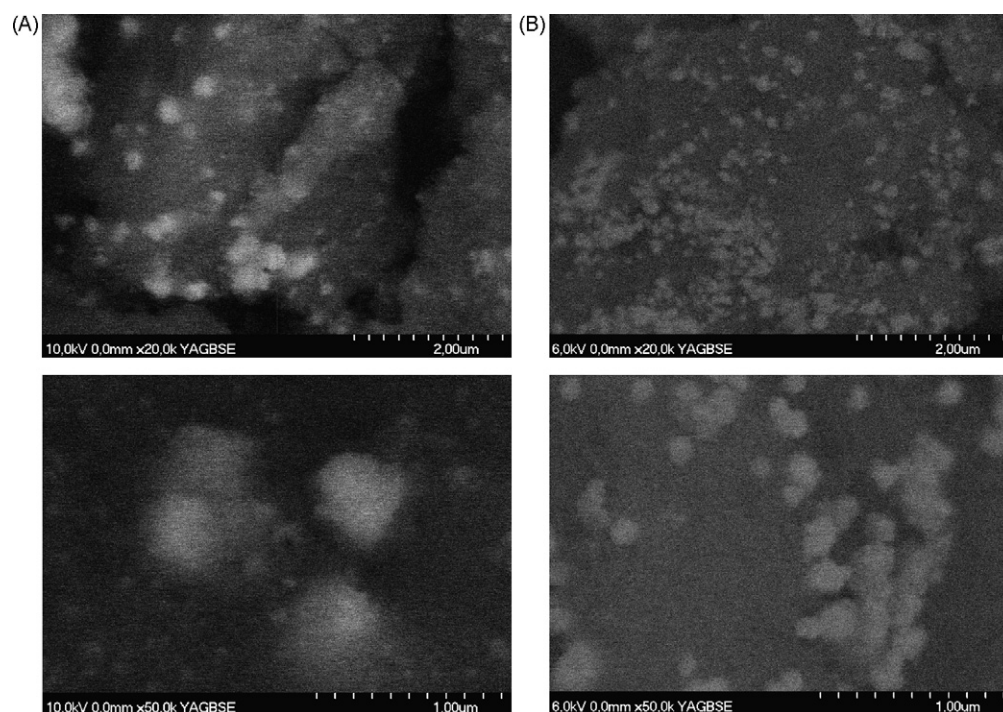


Fig. 11. SEM images of (A) 5Co + 15Mn and (B) 5Co15Mn-MS.

manganese catalysts (series B) occurs as Co^{2+} . (iii) Uniform distribution of the oxide agglomerates on the silica surface. The smallest crystal agglomerates are formed with the 5Co15Mn-MS sample. (iv) Formation of mixed Co–Mn oxide phases.

3.4.1. Catalytic activity

The temperature dependences of the complete *n*-hexane oxidation over the single and bicomponent catalysts are shown

in Figs. 12 and 13. H_2O and CO_2 were the only detectable reaction products in *n*-hexane oxidation on all the investigated samples from both series. As is evident from Figs. 12 and 13 the single component cobalt and manganese samples are active in the studied reaction. It is seen that the combustion activity of 15Mn is slightly lower than that of the cobalt sample. The addition of Mn to the calcined 15% Co/ SiO_2 sample leads to a decrease in the catalytic activity. XRD data show that the doping with Mn does not change

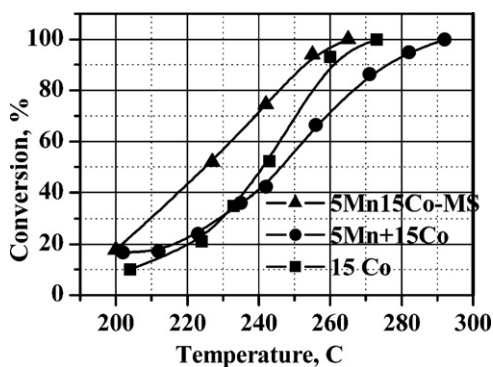


Fig. 12. Temperature dependence of *n*-hexane conversion over series A samples.

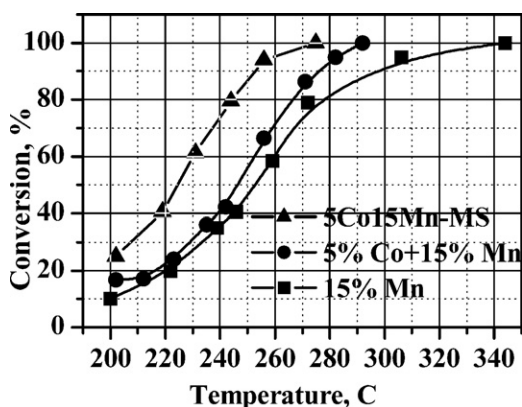


Fig. 13. Temperature dependence of *n*-hexane conversion over series B samples.

cobalt oxide particles size. Principal changes are associated with an increase in the temperature of Co_3O_4 reduction (TPR) and, according to XPS data, with a decrease in the Co/Mn atomic ratio at the surface. It is well known that transition metal oxides operate in complete hydrocarbon oxidation by a redox type mechanism, according to which the oxide species oxidize the hydrocarbon and is regenerated by the oxygen-containing gaseous phase. In this way, the catalytic behaviour can be correlated with the metal oxide reducibility. As is seen from the TPR data (Fig. 3), doping of the calcined single component cobalt sample with Mn leads to an increase in the reduction temperature of Co_3O_4 . An additional reason for the lower catalytic activity of the 5% Mn + 15% Co/ SiO_2 sample, in comparison with that of 15Co, is the decrease in the Co/Mn surface ratio. As was shown above, the lower Co/Mn ratio at the surface than that in the bulk can be explained by partial coverage of the cobalt oxide by manganese oxide that blocks some of the active cobalt sites in the reaction. A considerable increase in activity is established with the sample prepared from a mixed solution, 5Mn15Co-MS. This significant change in the catalytic activity can be ascribed to the following facts: (i) the formation of a finely divided cobalt oxide, which is reduced at a lower temperature, (ii) an enrichment in the Co component on the surface as demonstrated by XPS, and (iii) a uniform distribution of the oxide agglomerates on the silica surface, according to SEM images.

The dominating oxide phase in series B is manganese oxide. The 15Mn sample is less active than the other catalysts in the series. Doping with cobalt increases the catalytic activity and this depends on the sequence of active component introduction. The order of activity is as follows: 5Co15Mn-MS > 5Co + 15Mn > 15Mn. The decrease in the manganese oxide particle size and the enhancement of reducibility follow the same order as was shown by XRD and TPR data. The addition of Co to the calcined 15Mn sample causes a slight

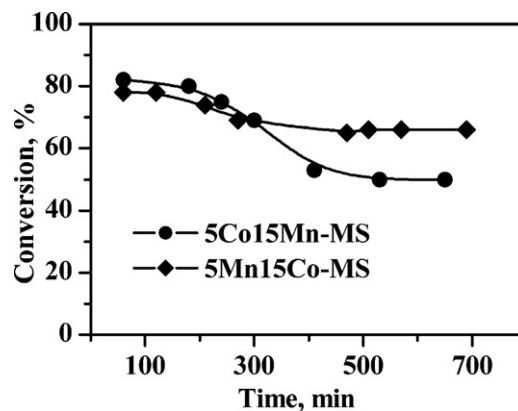


Fig. 14. *n*-Hexane conversion with time on stream over different samples.

increase in the catalytic activity. A considerable improvement in activity is established with the sample prepared from a mixed solution. The manganese oxides operate in the oxidation reactions through a Mars and van Krevelen mechanism and their redox properties play a key role. As is discussed above, the finely divided oxide particles are formed to a large extent in the 5Co15Mn-MS sample and, as a consequence, the reducibility of the oxide phase is enhanced. The increase in cobalt concentration on the support, as seen from XPS (Table 1), may be an additional reason for the enhancement of the activity, if we suggest that cobalt is more active species in the reaction of complete *n*-hexane oxidation. The SEM images demonstrate the smallest crystalline domains (100–200 nm size) with the 5Co15Mn-MS sample (Fig. 11). All the mentioned factors, the enrichment of the surface with Co, the considerable decrease in the metal oxide particle size, and the occurrence of small crystal agglomerates lead to an increase in the concentration of the catalytic active sites and an improvement in the catalytic activity.

Fig. 14 displays data on a stability test with the most active samples. The measurements were carried out at a temperature to give 80% initial conversion. For the bicomponent samples this temperature was 245 °C. The activity of the bicomponent samples dropped during time on stream and this was more significant for the sample in which the manganese oxide predominates. The decrease in catalytic activity can be correlated with sintering of the oxide phases. Particle size calculations according to XRD data on spent samples demonstrate that about a two-fold increase in the mean particle diameter of the bicomponent catalysts occurs during the stability test. For 5Mn15Co-MS the average particle size of Co_3O_4 increases from 7 nm before the reaction to 14 nm after the stability test (Table 1). The appearance of pure reflections for MnO_2 became evident from the XRD patterns of a spent 5Co15Mn-MS sample (not shown). The average particle size increases from 6.4 to 14 nm after the stability test. The 5Co15Mn-MS sample was chosen to evaluate the redox properties after the stability measurements. No appreciable changes in the redox properties could be detected with the spent catalyst, prepared from a mixed solution, with respect to the fresh one. This indicates that the redox features are quite stable under *n*-hexane oxidation. The observed slight shift to a higher reduction temperature is in accordance with an increase in the particle size.

4. Conclusions

Supported single component cobalt and manganese and bicomponent cobalt–manganese oxide catalysts are active in the complete oxidation of *n*-hexane. The catalytic activity of both single component cobalt and manganese samples is similar, however, a combination between the two elements changes significantly the activity and this depends on the method of

preparation. Addition of Mn to a calcined 15% Co/SiO₂ catalyst leads to a decrease in the catalytic activity in comparison with single cobalt. An increase in the reduction temperature of Co₃O₄ and a partial coverage of cobalt oxide by manganese oxide are the main factors responsible for low activity of the bicomponent sample. A slight increase in the catalytic activity after doping the calcined 15Mn sample with Co is a result of a decrease in MnO₂ particle size and a consequence of enhanced reducibility. A considerable increase in activity is established with all the samples prepared from a mixed solution, irrespective of the Co/Mn ratio. A very low crystallinity, partial enrichment of the surface with cobalt and a uniform distribution of oxides agglomerates on the support give rise to an increase in the concentration of the accessible active sites in these samples. The deactivation of the bicomponent samples could be a result of sintering of the oxide phase.

Acknowledgments

Authors would like to acknowledge the Bulgarian Academy of Sciences and Consejo Superior de Investigaciones Científicas (CSIC) for their support that made possible to carry out these investigations. The Spanish authors thank the Ministry of Science and Education of Spain for financial support (projects ENE2007-67926-C02-01 and P07-FQM-02520).

References

- [1] R. Craciun, B. Nentwick, K. Hadjiivanov, H. Knözinger, *Appl. Catal. A: Gen.* 243 (2003) 67–79.
- [2] Y.-F. Chang, J.G. McCarty, *Catal. Today* 30 (1996) 163–173.
- [3] R. Pereñíguez, J.L. Hueso, J.P. Holgado, F. Gaillard, A. Caballero, *Catal. Lett.* 131 (2009) 164–169.
- [4] J. Trawczyński, B. Bielak, W. Miśta, *Appl. Catal. B: Environ.* 55 (2005) 277–285.
- [5] M. Baldi, E. Finocchio, F. Milella, G. Busca, *Appl. Catal. B: Environ.* 16 (1998) 43–51.
- [6] M.C. Álvarez-Galván, B. Pawelec, V.A. de la Peña O'Shea, J.L.G. Fierro, P.L. Arias, *Appl. Catal. B: Environ.* 51 (2004) 83–91.
- [7] A. Gil, L.M. Gandía, S.A. Korili, *Appl. Catal. A: Gen.* 274 (2004) 229–235.
- [8] P. Papaefthimiou, Th. Ioannides, X.E. Verykios, *Appl. Catal. B: Environ.* 13 (1997) 175–184.
- [9] J.C. Wu, Z. Lin, F. Tsai, J. Pan, *Catal. Today* 63 (2000) 419–426.
- [10] J.C.-S. Wu, Z. Lin, J. Pan, M. Rei, *Appl. Catal. A: Gen.* 219 (2000) 117–124.
- [11] Y. Kalvachev, V. Kostov-Kytin, S. Todorova, K. Tenchev, G. Kadinov, *Appl. Catal. B: Environ.* 66 (2006) 192–197.
- [12] S. Todorova, G. Kadinov, K. Tenchev, Y. Kalvachev, V. Kostov-Kytin, *J. Mater. Sci.* 42 (2007) 3315–3320.
- [13] W. Li, Y. Lin, Y. Zhang, *Catal. Today* 83 (2003) 239–245.
- [14] W.B. Li, W.B. Chu, M. Zhuang, J. Hua, *Catal. Today* 93–95 (2004) 205–209.
- [15] P. Malet, A. Caballero, *J. Chem. Soc. Faraday Trans. 84* (1988) 2369–2371.
- [16] L. Lamaita, M.A. Peluso, J.E. Sambeth, H.J. Thomas, *Appl. Catal. B: Environ.* 61 (2005) 114–119.
- [17] S.B. Kanungo, *J. Catal.* 58 (1979) 419–435.
- [18] K.M. Parida, S.B. Kanungo, *Thermochim. Acta* 64 (1983) 131–138.
- [19] H.G. El-Shobaky, M.A. Shouman, A.A. Attia, *Colloid. Surf. A: Physicochem. Eng. Aspects* 274 (2006) 62–70.
- [20] F. Morales, D. Grandjean, F.M.F. de Groot, O. Stephanb, B.M. Weckhuysen, *Phys. Chem. Chem. Phys.* 7 (2005) 568–572.
- [21] F. Morales, E. de Smit, F.M.F. de Groot, T. Visser, B.M. Weckhuysen, *J. Catal.* 246 (2007) 91–99.
- [22] D. Shanke, S. Vada, E.A. Hilmen, A. Hoff, *J. Catal.* 156 (1995) 85–90.
- [23] M. Ferrandon, J. Carnö, S. Järäs, E. Björnborn, *Appl. Catal. A: Gen.* 180 (1999) 141–151.
- [24] F. Kapteijn, L. Singoredjo, A. Andreini, J.A. Moulijn, *Appl. Catal. B: Environ.* 3 (1994) 173–189.
- [25] Y. Okamoto, K. Nagata, T. Adach, T. Imanaka, K. Imamura, T. Takyu, *J. Phys. Chem.* 95 (1991) 310–319.
- [26] D. Das, G. Ravichandran, D.K. Chakrabarty, *Appl. Catal. A: Gen.* 131 (1995) 335–345.
- [27] E.R. Stobbe, B.A. de Boer, J.W. Geus, *Catal. Today* 47 (1999) 161–167.
- [28] T. Nissinen, M. Leskel, M. Gasik, J. Lamminen, *Thermochim. Acta* 427 (2005) 155–161.
- [29] G.C. Allen, K.R. Hallam, *Appl. Surf. Sci.* 93 (1996) 25–30.
- [30] J.L. Gautier, E. Rios, M. Gracia, J.F. Marco, J.R. Gancedo, *Thin Solid Films* 311 (1997) 51–57.
- [31] J.F. Moulder, W.F. Sticke, P.E. Sobol, K.D. Bombel, in: J. Castain (Ed.), *Handbook of X-ray Photoelectron Spectroscopy*, second edition, Perkin-Elmer Corporation, Physical Electron Division, Minnesota, USA, 1992.
- [32] G.L. Bezemer, P.B. Radstake, U. Falke, H. Oosterbeek, H.P.C.E. Kuipers, A.J. van Dillen, K.P. de Jong, *J. Catal.* 237 (2006) 152–161.
- [33] G.V. Bazuev, A.V. Korolyov, J. Magn. Mater. 320 (2008) 2267–2268.
- [34] A. Restovic, E. Rios, S. Barbato, J. Ortiz, J.L. Gautier, *J. Electroanal. Chem.* 522 (2002) 141–151.
- [35] R. Dula, R. Janik, T. Machej, J. Stoch, R. Grabowski, E.M. Serwicka, *Catal. Today* 119 (2007) 327–331.
- [36] T. Rao, M. Shen, L. Jia, J. Hao, J. Wang, *Catal. Commun.* 8 (2007) 1743–1747.